



Effect of two glycyrrhizinic acid nanoparticle carriers on MARC-145 cells actin filaments

Samantha Jardon¹ · Carlos G. García¹ · David Quintanar² · José L. Nieto¹ · María de Lourdes Juárez³ · Susana E. Mendoza⁴

Received: 2 February 2018 / Accepted: 29 March 2018 / Published online: 13 April 2018
© Springer-Verlag GmbH Germany, part of Springer Nature 2018

Abstract

The development of technologies that combine the advantages of nanomedicine with natural medicine represents a versatile approach to improve the safety and efficacy of drugs. Glycyrrhizinic acid (GA) is a natural compound that has a wide range of biological activities for the treatment of diseases. To establish a safe nanotransport system for this drug, two different nanoparticles with glycyrrhizinic acid, solid lipid nanoparticles (SLN–GA) and polymeric nanoparticles (PNP_S–GA) were elaborated to obtain nanostructure sizes between 200 and 300 nm. The nanoparticles were evaluated at concentrations of 1.25–100 µl/ml using the MARC-145 cell line to determine the effects on cell morphology, cellular structure (actin filaments) and cell viability (mitochondrial and lysosomal) at 24 and 72 h post-exposure. The safety range of the nanoparticles was 50 µl/ml, to determine that PNP_S–GA had an optimal safety profile and no cytotoxic effects, as there was no evidence of changes in morphology, internal cellular structures (stress fibers and the cell cortex formed by actin filaments) or viability under the experimental concentrations and conditions employed.

Keywords Solid lipid nanoparticles · Polymeric nanoparticles · Glycyrrhizin acid · Actin cytoskeleton · Morphologic changes · Cytotoxicity

Introduction

Application of nanotechnology to the health sciences has permitted the development of systems on the nanometric scale, which are denominated “nanoparticle drug carriers” (NPDC). These systems comprise at least two components; the first component is the active principle or the biologically

active molecule, and the second is the system which allows for a special function related to the diagnosis, treatment or prevention of disease (Irache and Nanomedicina 2008) (Fig. 1a).

The NPDC term includes nanocapsules and nanospheres. Nanocapsules are “vesicular systems” in which the drug is located inside of the particle and is usually dissolved in an oily vehicle. Nanospheres are “matrix-type” systems in which the drug is dispersed homogeneously into the constituent material (Olivier 2005) (Fig. 1a). These systems possess characteristics that determine their biological impacts, such as the chemical composition, size of the primary particle, morphology and solubility, among others. The advantages of using these systems is their ability to cross biological barriers and reach the organ, tissue or target cell group, arrive at intracellular compartments and control the release of the active molecule at its action or absorption site, thereby improving problems associated with the solubility, bioavailability, immunocompatibility and cytotoxicity of many drugs (Ramos et al. 2018; Kou et al. 2018; Jabr-Milane et al. 2008). NPDC with pharmaceutical purposes are mainly elaborated with polymers and lipids that are selected as raw material

✉ Susana E. Mendoza
seme_6@yahoo.com.mx

¹ Unidad de Investigación Multidisciplinaria L4 (Morfología Veterinaria y Biología Celular), UNAM-FESC, Campus 4, 54714 Cuautitlán Izcalli, Mexico

² Laboratorio de Investigación y Posgrado en Tecnología Farmacéutica, UNAM-FESC, Campus 1, 54714 Cuautitlán Izcalli, Mexico

³ Departamento de Morfología de la Facultad de Medicina Veterinaria y Zootecnia, UNAM-FMVZ, Mexico City, Mexico

⁴ Laboratorio de Virología y Microbiología de las Enfermedades Respiratorias del Cerdo, UNAM-FESC, Campus 1, 54714 Cuautitlán Izcalli, Mexico

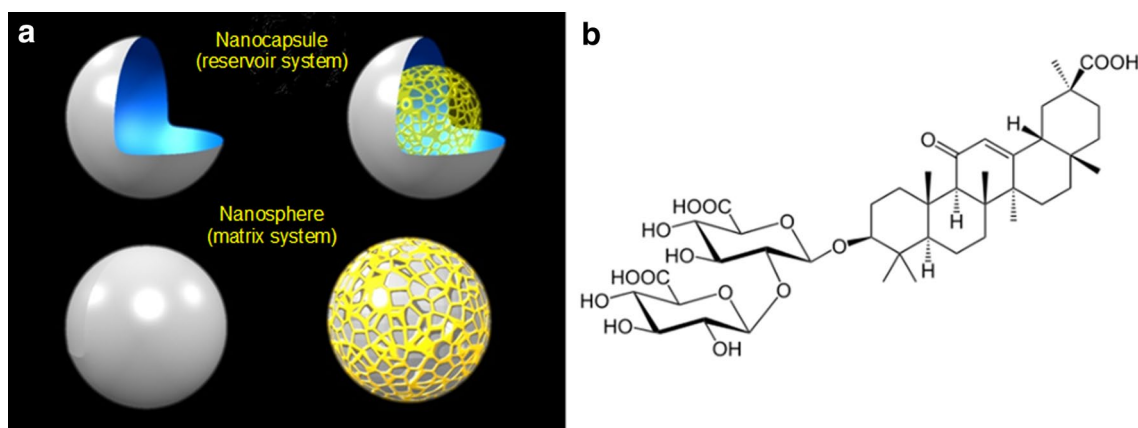


Fig. 1 **a** Drug nanotransporters and **b** the chemical structure of glycyrrhizinic acid

for the elaboration of the latter concern and are generally recognized as safe (GRAS) materials (Irache 2008).

Solid lipid nanoparticles (SLN) are considered prolonged release systems, due to possession of a solid nucleus stabilized with tensoactive or emulsifying elements (Urbán 2015, 2010). Müller et al. (2002) reported that although polymer nanoparticles (PNPs) were fabricated with polymers, the organism *in vivo* did not recognize them as foreign. Thus, PNPs are highly stable solid vectors that tend to encapsulate themselves in the interior of the capsule (Kumari et al. 2010). The development of these systems as a vehicle for active ingredients of natural origin for application in distinct diseases of interest in human and veterinary medicine is a promising field. Active ingredients of natural origin include glycyrrhizinic acid (GA) (Urbán 2015), which is a triterpenic saponin mainly responsible for the pharmacological activity of *Glycyrrhiza* species (Fig. 1b). In particular, the licorice plant (*Glycyrrhiza glabrata*), known as “sweet root”, is a legume found in sub-tropical regions that is recognized for its antiviral, antioxidant and antitumor properties, among others (Aguilar-Rosas et al. 2015; Izutani et al. 2014).

The development of novel drug administration systems should maintain a high safety range and permit the cells to monitor the environment and respond to external signals to survive. Vital physiological processes, such as cell division, adhesion, polarity, secretion, migration, changes in shape and ciliary and flagellar movement, are regulated by diverse signaling pathways and are executed through cytoskeletal reorganization (Liu et al. 2013). The cytoskeleton is a dynamic network composed of different proteins. The most predominant protein is actin, which possesses functions related to maintenance of the architecture and structural integrity of the cell; these functions are mainly associated with changes in shape and movement through structures, which is accomplished by filament rearrangements. Thus, the induction of changes in cell form and

migration in response to diverse extracellular signals is related to these filaments (Guirado et al. 2002). Actin presents in a globular/monomeric (G-actin) or filamentous/polymeric (F-actin) form. Actin monomers and filaments are attached to an important variety of proteins that regulate and modify their structures and functions. Actin filaments adopt distinct types of arrangements, such as bundles (parallel and contractile) and networks (mesh-like and dendritic). Parallel bundles are formed by actin filaments that are tightly associated and provide support to structures such as filopodia and microvilli. The contractile axes are composed of tightly associated antiparallel bundles of actin filaments and provide support for structures such as myosin (motor protein) that allows displacement of the filaments among them to form contractile structures, such as stress fibers or the muscular sarcomere. The mesh-formed networks comprise intertwined actin filaments and form the support for the lamellar part of the lamellipodia. The dendritic networks are composed of actin filaments that polymerize in a branched fashion and are found at the leading edge of the lamellipodia to produce membranous protrusions. The cell cortex is composed of a network of actin filaments bound to a plasma membrane. These actin filaments can be associated with myosin, which affords the cortex the capacity of contraction and tenses the filament network, rendering it more resistant and maintaining cell shape (Hotulainen and Lappalainen 2006; Cooper and Hausman 2009; Alberts 2014; Tojkander et al. 2012).

Because understanding the processes involved in exposure to NPDC is important, this work aimed to study the effects of two NPDC on the cell morphology, actin filament structure and internal cell activity of the MARC-145 cell line and to assess the possible therapeutic use of an active ingredient contained in nanotransporters. First, we performed actin cytoskeletal staining of control cultures at low and high confluence to establish the distribution of the actin filaments in these cells. Then, two different NPDC were

elaborated as the GA transport systems. Once the formulations were obtained, they were incubated with the cultures at concentrations ranging from 1.25 to 100 $\mu\text{g/ml}$ to determine changes in actin filament structure via a direct fluorescent technique and the integrity of the internal cellular activity through the thiazolyl blue [3-(4, 5-dimethylthiazol-2-yl)-2,5-diphenyltetrazolium bromide], neutral red and acridine orange assays.

Materials and methods

Glycyrrhizinic acid solutions

Glycyrrhizinic acid or ammonium salt (GA) (Sigma-Aldrich[®], 99% purity) was prepared from a 10 mg/ml stock solution of GA in RPMI medium. Dilutions were prepared to obtain the concentrations of the solutions employed in this work. All solutions were filtered through a 0.22- μm filter (Millipore[®]) under sterile conditions.

Nanoparticles preparation

The SLN were prepared by cooling the microemulsion as described by Urbán (2015) from 10% solid lipid fused lauroyl polyoxylglycerides (Gelucire 44/14 GATTEFOSSÉ), 1.5% surfactant poloxamer 407 (Pluronic F-127 cat. P2443) and 3% GA. The oleous phase was added with a slow flow in an excess of cold water (1:50) and dispersed with agitation at 1500 rpm in an IKA[®] RW20 shaker until the formation of lipid drops and their later precipitation was observed. Once the nanoparticles were obtained, they were separated by ultracentrifugation with two cycles at 50,000 rpm for 1 h in the Beckman-Coulter[®] LE-80K optimal ultracentrifuge; then, the SLN were resuspended in 1 ml of water. The PNPs were elaborated following the method described by Escalona (2017), which was a modification of the emulsification–diffusion technique described by Quintanar et al. (2005). The solvent was saturated by mixing water with ethyl acetate for 20 min; after separation, both phases were recovered independently and the interphase was discarded. Two grams of Mowiol 4–8 was dissolved in the aqueous phase with 1 ml of glacial acetic acid and 150 mg of chitosan. The aqueous and organic phases were mixed and centrifuged at 11,000 rpm for 10 min in an Ultraturax[®] equipment for the subsequent evaporation of the solvent in the Rotavapor for 1 h at 40 °C and 60 rpm. The PNPs were left to stabilize for 24 h and then centrifuged at 30,000 rpm for 30 min and resuspended in 2 ml of distilled water. Finally, the PNPs were added by slow flow to a 20 ml solution of water with 37 mg of GA. The formulation was maintained under magnetic agitation at 500 rpm for 1 h for absorption of the drug. In all

the preparations, the water employed was Milli-Q quality (Millipore[®], Bedford, MD, USA).

Nanoparticle drug carrier characterization

Partial particle size, polydispersion index and the Z potential

To determine the partial particle size (PPS), we employed the dynamic light scattering (DLS) technique (photon correlation spectroscopy, PCS) utilizing the Nanosizer[®] N4 Plus laser particle beam submicronic counter with laser beam dispersion at a 90 °C angle with a 680-nm wavelength for 180 s at 25 °C. The samples were diluted in distilled water until they corresponded to the sensitivity range of the apparatus. Dispersed-light data were analyzed using a digital correlator in unimodal analysis mode. Only formulations with a polydispersion index less than 0.5 were selected. The samples were analyzed at seven different time points post-elaboration on days 1, 2, 3, 4, 15 and 30. After the measurements were finalized, the samples were recovered for evaluation of the Z potential. These previous samples were subjected to Doppler laser microelectrophoresis in the Malvern[®] Zetasizer Nano HS, which employs an He/Ne laser beam 633 nm in length and 4 mW. We performed an average of 100 readings, and the determinations were conducted in triplicate.

Analysis of transmission scanning electron microscopy (SEM)

The samples were processed according to the method described by Quintanar et al. (2005). Following this method, the samples were placed on slides containing a 0.22 μm pore diameter membrane to dry at 25 °C. Then, the samples were covered with gold plating for 5 min at 7 amps in a Denton vacuum equipment for subsequent visualization at 25,000 \times in a JSM-6010LA model JEOL[®]-brand electron microscope.

In vitro evaluation in the cell line

Cell culture

We used the MARC-145 cell line (a clone of MA-104 African green monkey kidney cells). The cells were cultured in RPMI medium (Roswell Park Memorial Institute) medium supplemented with 10 and 5% fetal bovine serum (FBS) for the growth and maintenances phases, respectively, and penicillin/streptomycin (5000 IU/ml and 5 $\mu\text{g/ml}$, respectively). The cultures were maintained in a humidified incubator with a mixture of 95:5 air:CO₂ at 37 °C until the cells reached 90% confluence for use in the experiments. To detect changes in the cellular structure, the cells were cultured in

24-well microplates with previously sterilized 12-mm circular coverslips at a density of 1×10^5 cells per well.

Evaluation of the actin cytoskeleton and nuclei

To visualize the actin filaments and nuclei, we applied the direct fluorescent double-staining assay. The cells were fixed with 10% aqueous formalin in a phosphate-buffered saline (PBS) solution for 20 min and permeabilized with 0.5% Triton X-100 in PBS. To help reduce nonspecific binding, the cells were incubated with 1% bovine serum albumin (BSA) in PBS. To evaluate the actin filaments, the cells were incubated with tetramethyl rhodamine-isothiocyanate (TRITC)-labeled phalloidin (Sigma-Aldrich®) and diluted 1:100 in PBS for 20 min in a humid chamber in the dark. Then the cells were washed twice with PBS and once with deionized water. Finally, the coverslips were mounted onto slides using mounting medium with 4'-diamino-2-phenylindole (DAPI), to visualize the nuclei (Santa Cruz Biotechnology®, Santa Cruz, CA, USA). The slides were observed under the Zeiss® Axio scope 40 fluorescence microscope. The MARC-145 cell cultures were divided into groups that received different treatments as follows: GA (pure drug); SLN, PNP, SLN with GA (SLN-GA); and PNP with GA (PNPs-GA). For evaluation of the NPDC, we employed concentrations of 2.5, 5, 10, 25, 50 and 100 µg/ml. The positive control cells were exposed to 5 µl of 30 mM H₂O₂. The exposure times evaluated were 24 and 72 h.

Cytotoxicity assay

MTT assay For the thiazolyl blue [3-(4, 5-dimethylthiazol-2-yl)-2, 5-diphenyltetrazolium bromide] (MTT) assay, we incubated the cells with an MTT solution (0.5 mg/ml in each well) for 4 h in a humidified atmosphere with 5% CO₂ at 37 °C. Then the cells were lysed with 400 µl of dimethyl sulfoxide (DMSO). Finally, the intensity of the product was analyzed by spectrophotometry at 570 nm in a BioRad® model 550 microplate reader.

Neutral red assay The cells were incubated in a neutral red (NR) solution at a 33 µg/ml concentration in RPMI medium for 3 h at 37 °C; then, the colorant was removed, and the cells were washed with PBS. The colorant was extracted with a solution of acetic acid and ethanol (1:50), followed by agitation at room temperature (1:50) for 10 min. Finally, the absorbance was read at 540 nm. In each experiment, we utilized H₂O₂ (20 mM) as a positive control for cell death.

Acridine orange staining The cells were fixed with 4% paraformaldehyde in PBS for 10 min. Then, they were washed three times with PBS and incubated for 20 min in a 0.001% acridine orange solution in distilled water. Finally, the cells

were washed three times and directly observed under a fluorescence microscope.

Cellular uptake

First, 3 mg of coumarin 6 was dissolved in the AG absorption phase. The non-adsorbed fluorophore was removed by ultracentrifugation and washing in both methods. The cultures were exposed to 50 µl of SLN-GA and PNPs-GA with the fluorophore coumarin C6 for 4 h, and then processed as described for the direct fluorescence assay. Ten randomized fields per sample were captured and analyzed with the ImageJ® software. The nominal resolution of the images was 1 µm/5 pixels for the 40× objective for the Zeiss Axio scope 40® fluorescence microscope and 1 µm/2 pixels for the 10× objective with the UNICO® brand inverted microscope.

Statistical analysis

The data obtained from the experiments were analyzed independently based on a completely randomized design. Separation of media was effected by Tukey's test. The data were subjected to analysis of variance (ANOVA) utilizing the GraphPad Prism 7® statistical software package employing a significance level of $\alpha = 0.05$ to distinguish differences among groups. For the image analysis, we utilized the ImageJ® software.

Results

The SLN were prepared via microemulsion cooling according to the methodology described by Urbán (2015, 2010), whereas the PNPs were prepared using the emulsification-diffusion method described by Escalona (2017). Through the DLS technique, we determined that the SLN and PNPs presented nanometric sizes with maximal peak intensities at 280.31 ± 58.73 and 217.43 ± 11.44 nm, respectively, with a greater polydispersion index in the SLN than in the PNPs. However, this index was less than 1 in both systems, which was indicative of homogeneous sizes (Fig. 2a). The nanometric size was congruent with the micrographs, which evidenced structures inferior to micrometric size with the formation of a spherical-type morphology at 25,000× magnification (Fig. 2c, d). SLN without the drug are unstable systems that tend to agglomerate and form micrometric-sized structures from 96 h post-elaboration. In formulations with the drug, the stability period was maintained at the nanometric scale during the evaluation period and presented a slight increase in the particulate size that was directly proportional to the SLN elaboration time, thus

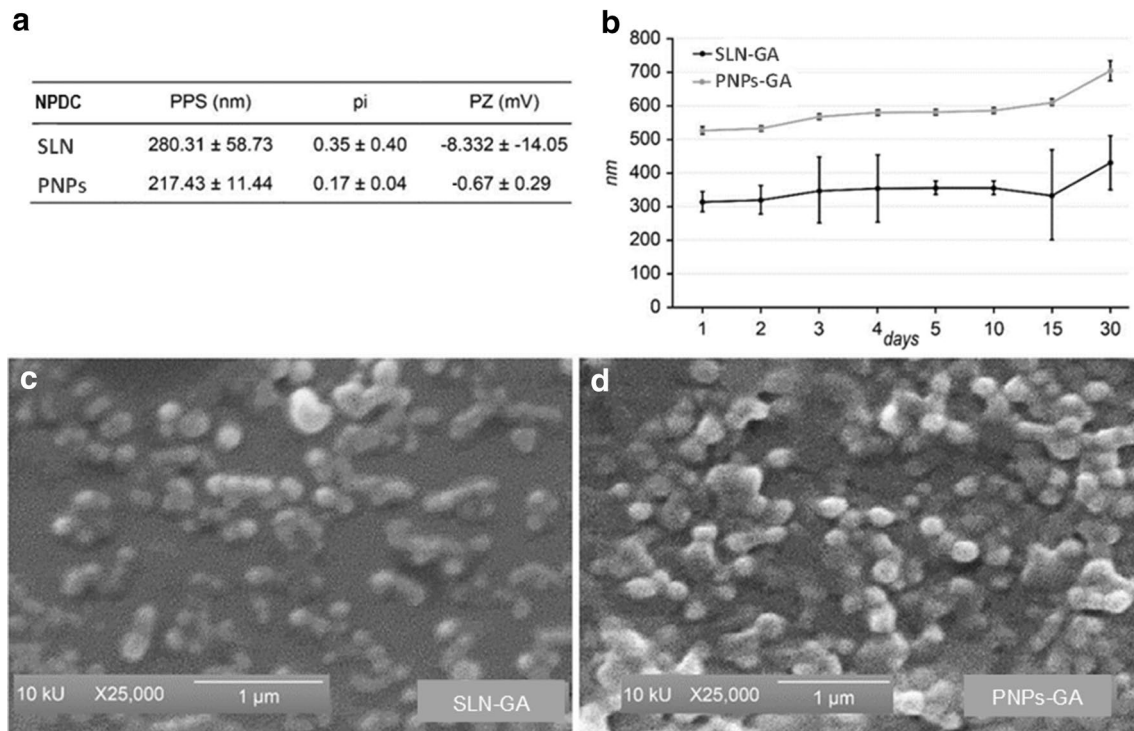


Fig. 2 Nanoparticle drug carrier characterization. **a** Average partial particulate size (PPS), polydispersion index and Z potential values of NPDC. **a** Graph of the size determination in the nanometric range of the SLN and PNPs via the DLS technique during a 30 day period at

ambient temperature. Scanning electron microscopic images taken at $\times 25,000$ magnification. Micrographs of the SLN-GA (**c**) and PNPs-GA (**d**). Bar = 1 μm

rendering the PNPs with a more stable system time. The storage conditions of the formulations were ambient temperature without protection from light (Fig. 2b).

To determine the effect of the NPDC on cellular morphology, we evaluated the actin cytoskeleton. MARC-145 cells showed a defined pattern of actin filaments that gave rise to diverse protrusive and contractile structures to provide strength to a series of vital cellular processes; these filaments extend from the perinuclear actin cap to the cortical region of the cell. Actin filaments form stress fibers that provide support to the cell and play an important role in mechanotransduction, which is a characteristic of cells that grow in rigid strata. The filaments are visible in MARC-145 cells, where they form radial longitudinal bundles and arcs (Fig. 3a). We observed a lamellipodia with an actin-enriched zone at the leading edge corresponding to a dendritic network (Fig. 3b). The actin pattern observed in a highly confluent culture showed a predominance at the cell cortex level and stress fibers spreading through the cytoplasm (Fig. 3c).

To evaluate the effects on the morphology and structure of MARC-145 cells exposed to 50 $\mu\text{l/ml}$ of the NPDC with and without the drug, the drug alone, and the controls (5% RPMI and 5 mM H_2O_2) for 24 h, we conducted direct double-staining fluorescent assays (actin filaments and nuclei).

Only the SLN treatment without the drug induced destruction of the monolayer, which severely affected the cellular morphology with a loss of the actin filament structure, whereas the PNPs treatment with and without the drug, the SLN treatment with the drug and the treatment with the pure drug maintained very similar cellular morphology patterns and actin filament structures compared to those of the control culture. We did not observe apparent cellular changes, because the cell cortex, lamellipodia and stress fiber structure were maintained; in addition to the presence of the cell cortex, the cells showed centric nuclei with a well-defined morphology (Fig. 4).

The cytotoxicity tests were performed by measuring the mitochondrial and lysosomal activity and evaluating nuclear integrity (Fig. 5). The MTT test demonstrated that the PNPs concentration range of 1.25–100 $\mu\text{l/ml}$ maintained viability above 70% compared to the control cells, similar to the results obtained with the NR assay (Fig. 5a, b). The SLN exhibited a lower margin of safety at concentrations greater than 50 $\mu\text{l/ml}$ of SLN-GA and 5 $\mu\text{l/ml}$ of SLN induced destruction of the cell monolayer integrity (Fig. 4). At doses lower than these ranges, the MTT test showed absorbances above the control that reflected an increase in viability when expressed as percentages. The MARC-145 cells were used

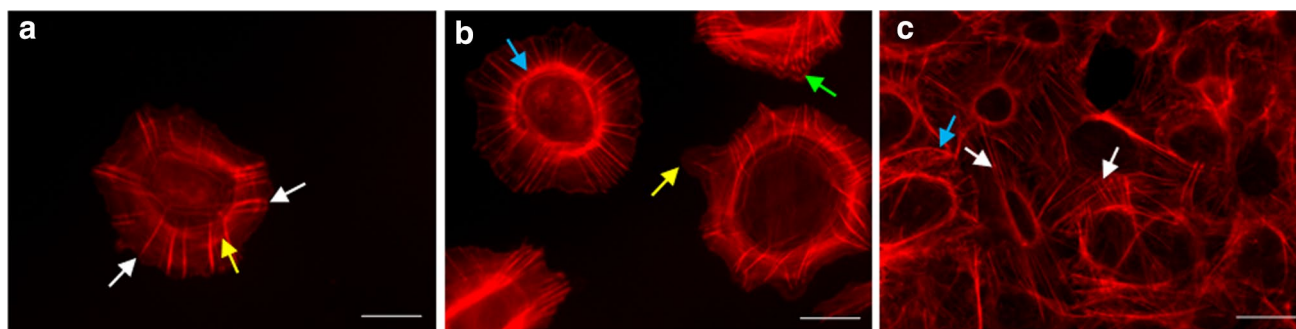


Fig. 3 Actin cytoskeleton in MARC-145 cells. Cell cultures at different stages of confluence. **a** The MARC-145 cells showed stress fibers with radial arrangement (white arrow) and the formation of arcs (yellow arrow). **b** The cells also showed the presence of lamellipodia (yellow arrow), as well as an actin-enriched zone corresponding to a dendritic network at the leading edge (green arrow) and a perinuclear

actin cap (blue arrow). **c** Stress fibers (white arrow) and the cell cortex (blue arrow) observed in a cell culture with 90% confluence. All cells shown are from cultures without treatment. Direct fluorescence assay, actin filaments stained with TRITC-labeled phalloidin. Fluorescence microscopy at $\times 40$ magnification. Bar = 10 μm

at 90% confluence for the cytotoxicity assays (Fig. 5c). MTT assay evidenced the formation of formazan crystals inside the cells from 1 h of exposure to MTT, until the end of incubation at 4 h (Fig. 5d, e).

SLN–GA induced nuclear damage at 72 h of exposure, with diminution of monolayer continuity (Fig. 6b), compared to the control cells (Fig. 6a); these results were congruent with those shown in Fig. 4. The PNP–GA did not evidence loss of cell and nuclear integrity under the same exposure scheme (Fig. 6c). The cellular internalization capacity of the systems was measured by fluorescence assays. During the elaboration of the NPDC, the fluorophore coumarin C6 was added, to assess the effects of acute exposure of the cultures for 4 h, and the actin cytoskeleton and nuclei were stained and observed under the fluorescence microscope. The SLN–GA and PNP–GA systems improved the cellular internalization processes measured indirectly by coumarin C6 displacement. The NPDC were detected in a pattern that suggested their internalization into cellular structures, and the staining was dependent on the exposure time. Coumarin C6-labeled SLN–GA and PNP–GA showed abundant staining on the periphery of the cell cytoplasm (Fig. 6e, f), which was in contrast to the culture exposed to medium containing coumarin C6, in which the fluorophore was distributed uniformly throughout the entire preparation (Fig. 6d).

Discussion

We centered our attention on the search for a nanoparticulate model that functioned as a vehicle for GA (Fig. 1a) GA is a component of natural origin that has been demonstrated to possess an antiviral effect (Baltina et al. 2009a, b; Aguilar-Rosas et al. 2015) against viruses such as influenza A (Harada 2005), herpes simplex virus type 1 (HSV-1), and

Newcastle virus (Baltina et al. 2009a, b; Pompei et al. 1979, 1980, 1983) and to diminish the viral replication of viruses such as severe acute respiratory syndrome (SARS) virus, as reported by Cinatl et al. (2003). Viral agents comprise a great challenge to human and animal health. One of the diseases with the greatest negative impact on the porciculture industry is reproductive and respiratory porcine syndrome (PRRS), which has been recognized by the authors including Albina (1997), Tian et al. (2007), Zimmerman et al. (2006) and Dea et al. (2000) as one of the diseases with the greatest negative economic impact worldwide. Kim et al. (1993) and Dea et al. (1995) reported a population derived from the MA-104 African green monkey kidney cell line than was highly permissive for replication of the PRRS virus (i.e., the MARC-145 cell line). Based on the results of the study, the MARC-145 cell line is considered the culture of choice for the replication of this pathogen. Urbán et al. (2015) described diminution of the infectivity of the PRRS virus due to treatment with GA in SLN; however, these authors did not conduct studies on the innocuousness of their transport system. The objective of this work was to establish a cellular model that allowed evaluation of the innocuousness of systems to examine the incorporation of drugs of natural origin into nanoparticulate models. These nanotransporters improve pharmacokinetics due to their nanometric sizes, which confer characteristics such as the ability to cross biological barriers and avoid premature degradation of the active ingredient, among other benefits described by authors such as Irache (2008). Not only is the size of the NPDC a desirable characteristic of these systems, but the nature of the materials with which they are elaborated also confer unique properties. SLN represent a good drug delivery system due to their lipophilic nature (Mehnert and Mäder 2001), as do PNPs, which are formed from polymers that are innocuous for living organisms (Escalona and

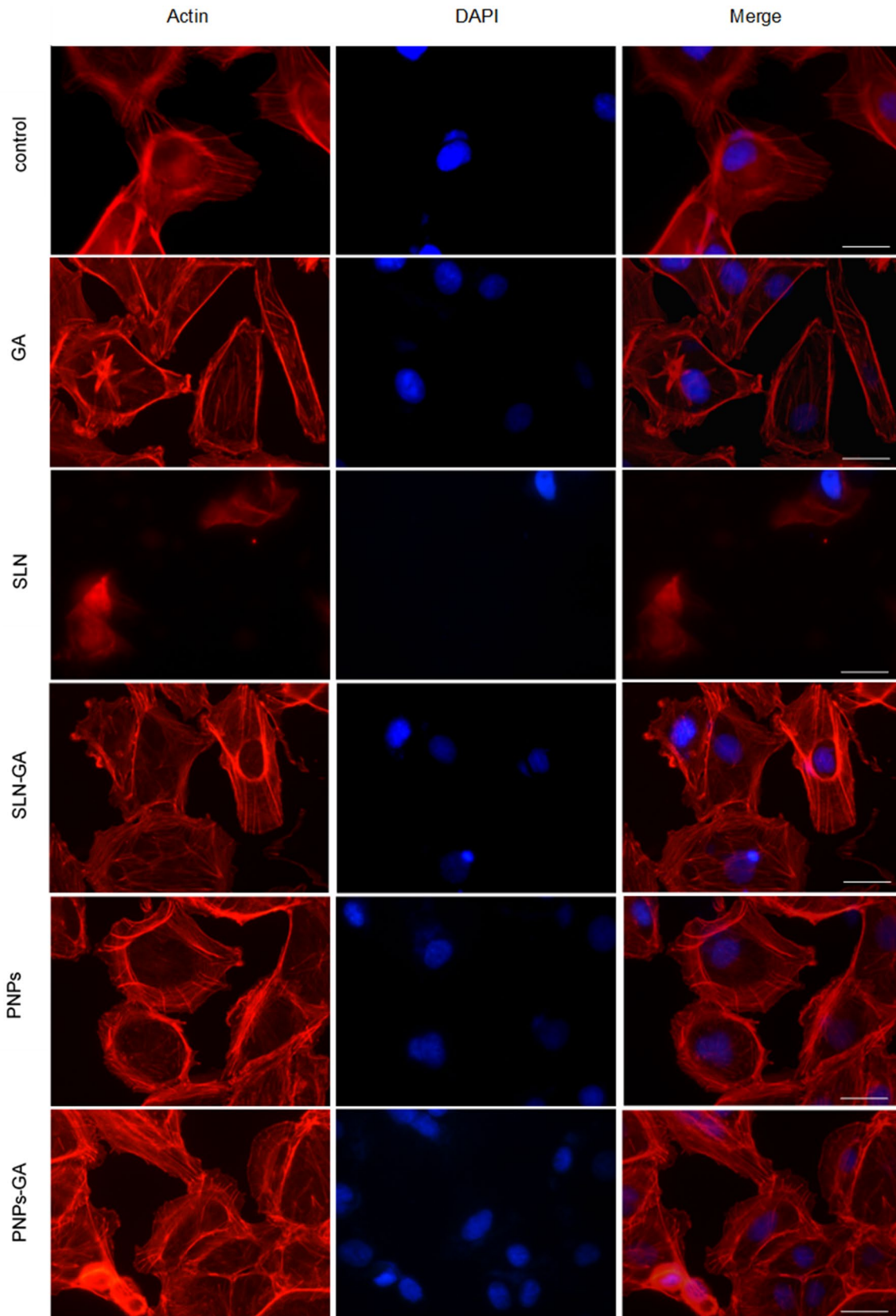


Fig. 4 Evaluation of the actin cytoskeleton to exposure to SLN and PNPs. The cultures were exposed for 24 h to the different treatments at an NPDC concentration of 50 $\mu\text{l/ml}$. The direct double-staining

fluorescent assay showed actin filaments stained with TRITC-labeled phalloidin and nuclei detected with DAPI. Fluorescence microscopy $\times 40$ magnification. Bar = 10 μm

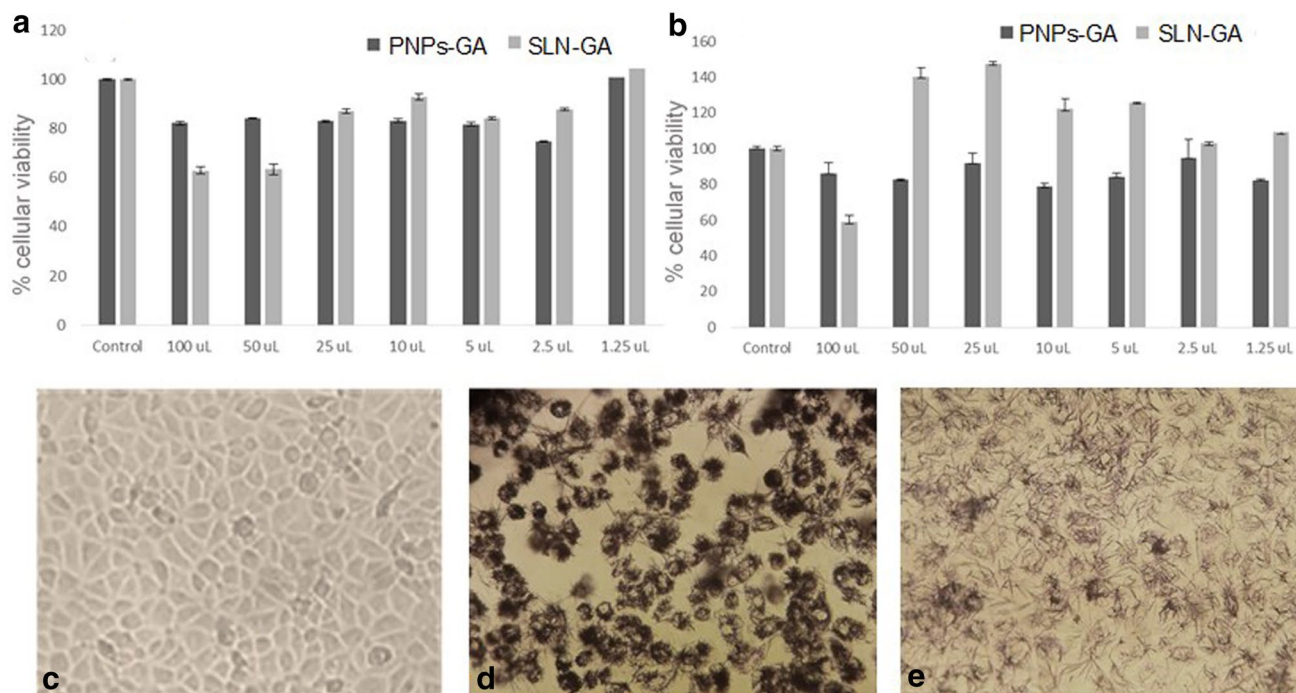


Fig. 5 SLN and PNPs cytotoxicity. **a** Measurement of mitochondrial activity with the MTT assay, **b** determination of lysosomal activity with the neutral red assay. Graphs expressed in percentages compared to the controls for each treatment. Data were obtained from three

independent experiments. ANOVA. *** $p < 0.001$, cells; ** $p < 0.01$, and * $p < 0.05$. **c** Formazan crystal formation in MARC-145 control cell compared to MARC-145 cells exposed to SLN-GA (**d**) and PNPs-GA (**e**). Bar = 100 μ m

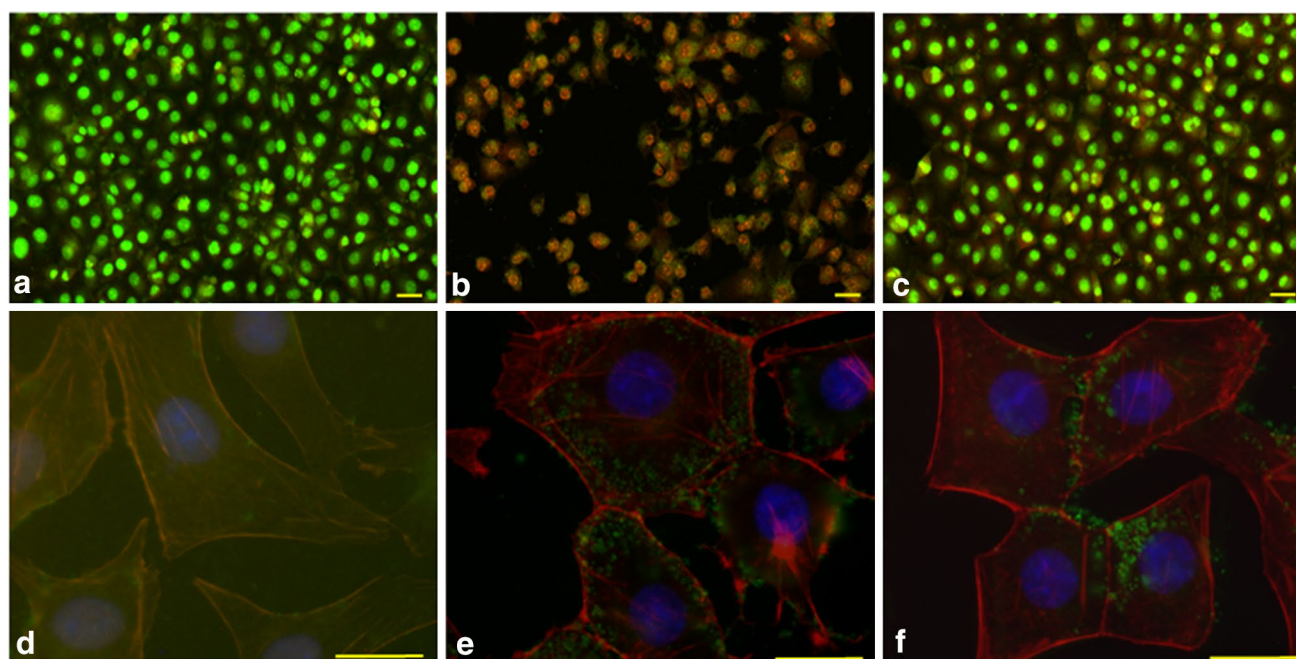


Fig. 6 Nuclear integrity and cellular uptake of NPDC. Cultures of MARC-145 cells were exposed to NPDC with the drug for 24 h, followed by acridine orange staining to evaluate the effect on nuclear integrity. **a** Control, **b** SLN-GA, **c** PNPs-GA. Fluorescence micros-

copy, $\times 20$ magnification. Internalization of NPDC into the cells at 4 h of exposure based on coumarin C6 staining. **d** Medium-free coumarin C6, **e** coumarin C6-labeled SLN-GA, **f** coumarin C6-labeled PNPs-GA. Fluorescence microscopy, $\times 40$ magnification. Bar = 50 μ m

Quintanar 2014). However, to the best of our knowledge, no information is available on the mechanism of action and the effects of these particles on cellular structure and internal cellular activity.

We assessed actin filaments to evaluate the structural integrity of the cells. In MARC-145 cells, actin filaments presented a clear definition and disposition of the stress fibers characteristic of relatively stable cells that grew in rigid strata (Pellegrin and Mellor 2007; Pollard 2007; Tojkander et al. 2012). The pattern of actin in highly confluent cultures manifests predominance at the cell cortex level with stress fibers spreading through the cytoplasm, suggesting important regulation of the cell form and its participation in the formation of cell junctions and focal adhesions as well as participation in signaling pathways (Khatau et al. 2009).

The safety ranges of SLN and PNPs with and without the drug were determined by the MTT and NR assays. The PNPs systems with and without the drug possessed a greater safety range. SLN without the drug were the most cytotoxic system, with very low safety margins (i.e., 5 µg/ml). The addition of GA raises the dose to a maximal range of 50 µg/ml at 24 h of exposure as measured by mitochondrial and lysosomal activity; this finding suggests that the lipid concentration is crucial for establishing safety. Additionally, the latter finding indicates that the presence of high lipid contents permits abrupt fusion with the cell membrane, causing severe osmotic disequilibria and cell death, due to induction of actin filament depolymerization, with a resultant loss of stress fiber and the cell cortex structure and subsequent nuclear destruction (Fig. 4). The drug is adsorbed inside the NPDC, where it occupies space in its structure with sufficient effectiveness to diminish the lipid concentration and permit maintenance of the SLN–GA with a tenfold greater safety margin. Therefore, for SLN, the therapeutic margin should be standardized for the transport of other drugs. At doses less than 50 µg/ml, neither system affects the cellular morphology and actin filament structure. The mitochondrial and lysosomal activities were greater than 80%, suggesting that no cell damage occurred (Fig. 5a, b). For PNPs with and without the drug, there is no evidence of diminution of cell viability under 80% compared to the control within the 100–1.25 µg/ml concentration range. The PNPs nanotransporters exhibited less toxicity, which could be related with their smaller sizes (Fig. 2a). Katsumiti et al. (2015) reported the presence of PPS-dependent cytotoxic effects measured by the MTT and NR assays. Mitochondrial activity results in reduction of methyl tetrazolium into formazan via the mitochondrial enzyme succinate dehydrogenase, which is increased in the presence of SLN. Formazan is a membrane-impermeable compound; thus, it accumulates in the interior of healthy cells and is easily observed by bright-field microscopy (Fig. 5d, e), as reported by authors such as Mossman (1983) and Fotakis and Timbrell (2006). Formazan is a

strongly lipophilic substance; therefore, the presence of the needle-shaped crystals of formazan is increased inside cells treated with SLN–GA, suggesting optimal internalization of the nanoparticulate systems, as described by Angius and Floris (2015).

During elaboration of the NPDC, they were conjugated with the fluorophore coumarin C6. To evaluate internalization of the NPDC, the cell cultures were acutely exposed to coumarin C6-labeled NPDC for 4 h. We evaluated internalization of NPDC, as well as the actin cytoskeleton and nuclear integrity through fluorescence microscopy. The coumarin C6-conjugated NPDC allowed visualization of the degree of internalization in the cells; thus, internalization of the NPDC conjugated with coumarin C6 could be estimated based on displacement inside the cells by observing the fluorescence emitted by the coumarin C6. Coumarin C6-labeled SLN–GA and PNPs–GA showed fluorescent staining in the cell cytoplasm (Fig. 6e, f). The absence of coumarin C6-labeled NPDC throughout the entire existing space among the cells is suggestive of the uptake of the NPDC systems inside the cells. In cells treated with SLN–GA, we observed a predominance of staining that was distributed more profusely in the cytoplasm, and PNPs were observed to a greater degree toward the periphery. NPDC appear to be facilitator systems for the drug, because the detection of coumarin C6-labeled NPDC in the cells revealed a pattern dependent upon the time of exposure. These data were similar to the results observed by Kim et al. (2016), who reported the presence of positive fluorescence in the interior of Caco-2 cells exposed to fluorescein isothiocyanate (FITC)-labeled NPDC for 4 h. These results suggest that SLN and PNPs can be employed as GA-supplier systems. In the assay with coumarin C6-labeled NPDC, the drug internalization process did not cause alterations in cellular morphology or in the actin cytoskeleton structure, measured indirectly by coumarin C6 displacement. However, confocal microscopy studies should be conducted to establish a three-dimensional (3D) reconstruction of the cells using distinct optical cuts to determine the exact site where the stain is concentrated.

Conclusions

The cooling of microemulsion and emulsification–diffusion methods are optimal for obtaining homogeneous and spherical nanometric-dimension structures that are lipidic and polymeric in nature. These structures are employed as nanotransporters for glycyrrhizic acid. The structures did not affect MARC-145 cell integrity and viability at doses lower than 50 µl/ml, because we did not observe changes in actin filament structures or in mitochondrial and lysosomal activity. Acridine orange staining suggests that polymeric nanoparticles comprise an innocuous system that is

superior to lipid nanoparticles at 72 h of exposure under the conditions evaluated in the present investigation. Using assays with coumarin C6-labeled NPDC, we corroborated the internalization of GA transported by the NPDC, which suggested a facilitator role for crossing the cell membrane and internal transport. MARC-145 cells represented a good model for evaluation of the morphological, structural and functional integrity of the cells through the determination of rearrangements and modification in the actin cytoskeleton and internal cell activity, the latter with the aim of assessing the effects induced by the NPDC. The results will be highly useful for later works evaluating the antiviral effects of GA transported by NPDC.

Acknowledgements We are grateful to the Consejo Nacional de Ciencia y Tecnología (CONACYT) for grant # 486348/282140, awarded perform doctoral studies and for projects PIAPI 001, PIAPI 1602 and PIAPI 1655 (FESC-UNAM), CONACYT CB-221629, CONACYT INFRA 251940, and PAPITT IN18516 (DGAPA-UNAM). Thanks to M.C. Francisco Rodolfo González Díaz and M.C. Sofía González Gallardo, for their technical support during the realization of this work; and to laboratory 6 of the Unidad de Investigación Multidisciplinaria for facilitate the use of fluorescence microscope.

Compliance with ethical standards

Conflict of interest The authors of this manuscript do not have any conflicts of interest related to the information cited herein.

References

- Aguilar-Rosas I, Alcalá-Alcalá S, Llera-Rojas V, Ganem-Rondero A (2015) Preparation and characterization of mucoadhesive nanoparticles of poly (methyl vinyl ether-*co*-maleic anhydride) containing glycyrrhizic acid intended for vaginal administration. *Drug Dev Ind Pharm* 41:1632–1639. <https://doi.org/10.3109/03639045.2014.980425>
- Alberts B (2014) *Molecular biology of the cell*, 6th edn. Garland Science, New York
- Albina E (1997) Epidemiology of porcine reproductive and respiratory syndrome (PRRS): an overview. *Vet Microbiol* 55:309–316. [https://doi.org/10.1016/S0378-1135\(96\)01322-3](https://doi.org/10.1016/S0378-1135(96)01322-3)
- Angius F, Floris A (2015) Liposomes and MTT cell viability assay: an incompatible affair. *Toxicol In Vitro* 29:314–319. <https://doi.org/10.1016/j.tiv.2014.11.009>
- Baltina LA, Kondratenko RM, Baltina LA, Baschenko NZ, Plyasunova OA (2009a) Synthesis and biological activity of new glycyrrhizic acid conjugates with amino acids and dipeptides. *Russ J Bioorg Chem* 35:510–517. <https://doi.org/10.1134/S1068162009040141>
- Baltina LA, Kondratenko RM, Baltina LA, Plyasunova OA, Pokrovskii AG, Tolstikov GA (2009b) Prospects for the creation of new antiviral drugs based on glycyrrhizic acid and its derivatives (a review). *Pharm Chem J* 43:539–548. <https://doi.org/10.1007/s11094-010-0348-2>
- Cinatl J, Morgenstern B, Bauer G, Chandra P, Rabenau H, Doerr HW (2003) Glycyrrhizin, an active component of liquorice roots, and replication of SARS-associated coronavirus. *Lancet* 361:2045–2046. [https://doi.org/10.1016/S0140-6736\(03\)13615-X](https://doi.org/10.1016/S0140-6736(03)13615-X)
- Cooper GM, Hausman RE (2009) *Cell death and cell renewal. The cell: a molecular approach*. Sinauer and Associates, Sunderland, pp 693–722
- Dea S, Sawyer N, Alain R, Athanassios R (1995) Ultrastructural characteristics and morphogenesis of porcine reproductive and respiratory syndrome virus propagated in the highly permissive MARC-145 cell clone. *Adv Exp Med Biol* 380:95–98. https://doi.org/10.1007/978-1-4615-1899-0_13
- Dea S, Gagnon CA, Mardassi H, Pirzadeh B, Rogan D (2000) Current knowledge on the structural proteins of porcine reproductive and respiratory syndrome (PRRS) virus: comparison of the North American and European isolates. *Arch Virol* 145:659–688. <https://doi.org/10.1007/s007050050662>
- Escalona RO (2017) *Desarrollo y caracterización de nanopartículas con superficie modificada Como potenciales transportadores de fármacos a través de la barrera hematoencefálica*. Tesis Maestría. Programa de Maestría y Doctorado en Ciencias Químicas. Universidad Nacional Autónoma de México, México
- Escalona RO, Quintanar GD (2014) Nanogeles poliméricos: una nueva alternativa para la administración de fármacos. *Rev Mex Cienc Farm* 45:17–38
- Fotakis G, Timbrell JA (2006) In vitro cytotoxicity assays: comparison of LDH, neutral red, MTT and protein assay in hepatoma cell lines following exposure to cadmium chloride. *Toxicol Lett* 160:171–177. <https://doi.org/10.1016/j.toxlet.2005.07.001>
- Guirado BO, Solanas GM, Costa TI, Escrich EE (2002) El citoesqueleto de actina: una perspectiva desde la biología molecular del cáncer. *Rev Cuba Invest Biomed* 21:115–122
- Harada S (2005) The broad anti-viral agent glycyrrhizin directly modulates the fluidity of plasma membrane and HIV-1 envelope. *Biochem J* 392:191–199. <https://doi.org/10.1042/BJ20051069>
- Hotulainen P, Lappalainen P (2006) Stress fibers are generated by two distinct actin assembly mechanisms in motile cells. *J Cell Biol* 173:383–394. <https://doi.org/10.1083/jcb.200511093>
- Irache JM (2008) In *Nanomedicina nanopartículas con aplicaciones médicas*. *Anal Sist Sanit Navar SciELO Esp* 31–1:7–10
- Izutani Y, Kanaori K, Oda M (2014) Aggregation property of glycyrrhizic acid and its interaction with cyclodextrins analyzed by dynamic light scattering, isothermal titration calorimetry, and NMR. *Carbohydr Res* 392:25–30. <https://doi.org/10.1016/j.carres.2014.04.017>
- Jabr-Milane L, Van Vlerken L, Devalapally H, Shenoy D, Komareddy S, Bhavsar M, Amiji M (2008) Multi-functional nanocarriers for targeted delivery of drugs and genes. *J Control Release* 130:121–128. <https://doi.org/10.1016/j.jconrel.2008.04.016>
- Katsumiti A, Gilliland D, Arostegui I, Cajaraville MP (2015) Mechanisms of toxicity of Ag nanoparticles in comparison to bulk and ionic Ag on mussel hemocytes and gill cells. *PLoS ONE* 10:e0129039. <https://doi.org/10.1371/journal.pone.0129039>
- Khataou SB, Hale CM, Stewart-Hutchinson PJ, Patel MS, Stewart CL, Searson PC, Hodzic D, Wirtz D (2009) A perinuclear actin cap regulates nuclear shape. *Proc Natl Acad Sci USA* 106:19017–19022. <https://doi.org/10.1073/pnas.0908686106>
- Kim HS, Kwang J, Yoon IJ, Joo HS, Frey ML (1993) Enhanced replication of porcine reproductive and respiratory syndrome (PRRS) virus in a homogeneous subpopulation of MA-104 cell line. *Arch Virol* 133:477–483. <https://doi.org/10.1007/BF01313785>
- Kim JH, Park EY, Ha HK, Jo CM, Lee WJ, Lee SS, Kim JW (2016) Resveratrol-loaded nanoparticles induce antioxidant activity against oxidative stress. *Asian-Australas J Anim Sci* 29:288–298. <https://doi.org/10.5713/ajas.15.0774>
- Kou L, Bhitia YD, Yao Q, He Z, Sun J, Ganapathy V (2018) Transporter-guided delivery of nanoparticles to improve drug permeation across cellular barriers and drug exposure to selective cell types. *Front Pharmacol* 9:27

- Kumari A, Yadav SK, Yadav SC (2010) Biodegradable polymeric nanoparticles based drug delivery systems. *Colloids Surf B Biointerfaces* 75(1):1–18
- Liu C, Fallen MK, Miller H, Upadhyaya A, Song W (2013) The actin cytoskeleton coordinates the signal transduction and antigen processing functions of the B cell antigen receptor. *Front Biol* 8:475–485. <https://doi.org/10.1007/s11515-013-1272-0>
- Mehnert W, Mäder K (2001) Solid lipid nanoparticles: production, characterization and applications. *Adv Drug Deliv Rev* 47:165–196. [https://doi.org/10.1016/S0169-409X\(01\)00105-3](https://doi.org/10.1016/S0169-409X(01)00105-3)
- Mosmann T (1983) Rapid colorimetric assay for cellular growth and survival: application to proliferation and cytotoxicity assays. *J Immunol Methods* 65:55–63. [https://doi.org/10.1016/0022-1759\(83\)90303-4](https://doi.org/10.1016/0022-1759(83)90303-4)
- Müller RH, Radtke M, Wissing SA (2002) Nanostructured lipid matrices for improved microencapsulation of drugs. *Int J Pharm* 242(1–2):121–128
- Olivier JC (2005) Drug transport to brain with targeted nanoparticles. *NeuroRx* 2(1):108–119
- Pellegrin S, Mellor H (2007) Actin stress fibres. *J Cell Sci* 120:3491–3499. <https://doi.org/10.1242/jcs.018473>
- Pollard TD (2007) Regulation of actin filament assembly by Arp2/3 complex and formins. *Annu Rev Biophys Biomol Struct* 36:451–477. <https://doi.org/10.1146/annurev.biophys.35.040405.101936>
- Pompei R, Flore O, Marccialis MA, Pani A, Loddo B (1979) Glycyrrhizic acid inhibits virus growth and inactivates virus particles. *Nature* 281:689–690. <https://doi.org/10.1038/281689a0>
- Pompei R, Pani A, Flore O, Marccialis MA, Loddo B (1980) Antiviral activity of glycyrrhizic acid. *Experientia* 36:304. <https://doi.org/10.1007/BF01952290>
- Pompei R, Paggi L, Ingianni A, Uccheddu P (1983) Glycyrrhizic acid inhibits influenza virus growth in embryonated eggs. *Microbiologica* 6:247–250
- Quintanar-Guerrero D, Tamayo-Esquivel D, Ganem-Quintanar A, Allémann E, Doelker E (2005) Adaptation and optimization of the emulsification-diffusion technique to prepare lipidic nanospheres. *Eur J Pharm Sci* 26:211–218. <https://doi.org/10.1016/j.ejps.2005.06.001>
- Ramos MA, Da Silva PB, Spósito L, De Toledo LG, Bonifácio BV, Rodero CF, Bauab TM (2018) Nanotechnology-based drug delivery systems for control of microbial biofilms: a review. *Int J Nanomed* 13:1179
- Tian K, Yu X, Zhao T, Feng Y, Cao Z, Wang C, Hu Y, Chen X, Hu D, Tian X, Liu D, Zhang S, Deng X, Ding Y, Yang L, Zhang Y, Xiao H, Qiao M, Wang B, Hou L, Wang X, Yang X, Kang L, Sun M, Jin P, Wang S, Kitamura Y, Yan J, Gao GF (2007) Emergence of fatal PRRSV variants: unparalleled outbreaks of atypical PRRS in China and molecular dissection of the unique hallmark. *PLoS ONE* 2:e526. <https://doi.org/10.1371/journal.pone.0000526>
- Tojkander S, Gateva G, Lappalainen P (2012) Actin stress fibers—assembly, dynamics and biological roles. *J Cell Sci* 125:1855–1864. <https://doi.org/10.1242/jcs.098087>
- Urbán MZ (2015) Evaluación de la actividad terapéutica del ácido glicirricínico formulado en sistemas submicrónicos contra el virus de PRRS. Tesis doctoral. Universidad Nacional Autónoma de México, México
- Zimmerman J, Benfield DA, Murtaugh MP, Osorio F, Stevenson GW, Torremorell M (2006) Porcine reproductive and respiratory syndrome virus (porcine arterivirus). *Dis Swine* 9:387–418

Publisher's Note Springer Nature remains neutral with regard to jurisdictional claims in published maps and institutional affiliations.